Fast FE-Analysis and Measurement of the Hydraulic Transfer Function of Pipes with Non-Uniform Cross Section

J. Herrmann, M. Spitznagel, L. Gaul
Institute of Applied and Experimental Mechanics, University of Stuttgart, Germany
Email: {herrmann,gaul}@iam.uni-stuttgart.de

Introduction

Automotive piping systems are often characterized by a non-uniform cross section. Orifices in fuel charge assemblies are a typical example. The goal of this research is to quantify the influence of diameter changes on the hydraulic transfer function of the pipe. A finite element based substructuring and component mode synthesis technique [1, 2] is used to assemble the spatial piping system including the orifice. The adaptation of the Craig-Bampton method to fluid-structure coupled piping systems with an additional reduction of the remaining interface degrees of freedom leads to a considerable model order reduction and computational speedup [3]. A local, frequency dependend fluid damping model [4] is integrated in the finite element code and the result of the harmonic analysis is compared to measurements. A hydraulic test bench with a dynamic pressure source [5] is used to estimate the hydraulic transfer function for different orifice diameters.

Finite Element Modeling of Fluid-Filled Piping System

The substructures of the spatial piping assembly are modeled using the finite element method. The discretized fluid and structural partitions are coupled by a fluid-structure interface [6]. Two coupling conditions hold, namely the Euler equation and the reaction force axiom at the fluid-structure interface. A finite element formulation based on the principle of virtual displacements [6] leads to coupled discretized equations in terms of nodal structural displacements $\boldsymbol{u}$ and nodal acoustic excess pressure $\boldsymbol{p}$

$$\underbrace{\begin{bmatrix} \boldsymbol{M}_\mathrm{s} & \boldsymbol{0} \\ \rho_0 \boldsymbol{C}^T & \boldsymbol{M}_\mathrm{a} \end{bmatrix}}_{\boldsymbol{M}\in\mathbb{R}^{n\times n}} \begin{bmatrix} \ddot{\boldsymbol{u}} \\ \ddot{\boldsymbol{p}} \end{bmatrix} + \underbrace{\begin{bmatrix} \boldsymbol{K}_\mathrm{s} & -\boldsymbol{C} \\ \boldsymbol{0} & \boldsymbol{K}_\mathrm{a} \end{bmatrix}}_{\boldsymbol{K}\in\mathbb{R}^{n\times n}} \begin{bmatrix} \boldsymbol{u} \\ \boldsymbol{p} \end{bmatrix} = \begin{bmatrix} \boldsymbol{f}(t) \\ \boldsymbol{q}(t) \end{bmatrix}. \quad (1)$$

Note that index "s" denotes the structural partition, whereas index "a" characterizes the acoustical fluid. The discretized equations include mass and stiffness matrices $\boldsymbol{M}_{\mathrm{s,a}}$ and $\boldsymbol{K}_{\mathrm{s,a}}$, respectively, as well as the coupling matrix $\boldsymbol{C}$. A cut through the discretized FE-model of the substructure with a cross section change is shown in Fig. 1. The next section gives insight in the efficient substructuring technique to assemble the piping system.

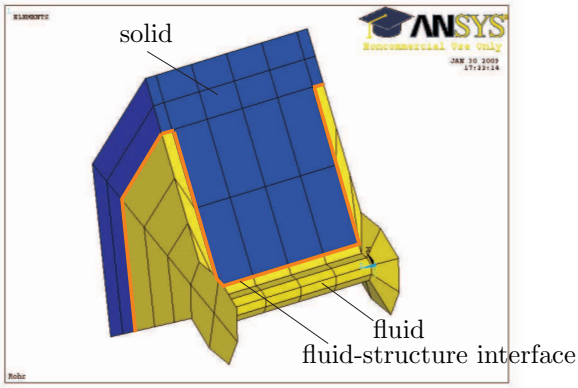

Figure 1: Cut through the discretized substructure with the cross section change.

Substructuring and Model Reduction

According to the Craig–Bampton method [1], a transformation with respect to the component interface degrees of freedom is followed by a model reduction in modal space. The reduction basis consists of constraint modes characterizing the static solution and fixed interface modes up to a certain frequency of interest. The Craig–Bampton method maintains the full number of DOFs at the interface. However, the associated model partition includes high–frequency dynamic content, which is not needed in a final reduced substructure model. For this reason, an interface reduction method is applied to the substructure models received so far. Appropriate sets of Ritz vectors are determined to build the interface reduction bases $\boldsymbol{\Delta}_\mathrm{s}$ and $\boldsymbol{\Delta}_\mathrm{a}$, such that the relevant dynamic deflections and the acoustic pressure field on the interface is approximated well at low–frequencies. The first set of Ritz vectors are eigenvectors from the local eigenvalue problem determined by the interface partition of mass and stiffness matrix as proposed by Craig and Chang [7]. It is important to augment these local interface eigenvectors by additional sets of Ritz vectors, namely the interface partition of rigid body and low–frequency modes computed from the eigenvalue problem of the free–floating substructure [3]. Finally, the overall reduction bases are given as

$$\begin{bmatrix} \boldsymbol{u}_\mathrm{I} \\ \boldsymbol{u}_\mathrm{F} \end{bmatrix} = \begin{bmatrix} \boldsymbol{\Delta}_\mathrm{s} & \boldsymbol{0} \\ -\boldsymbol{K}_{\mathrm{s,FF}}^{-1}\boldsymbol{K}_{\mathrm{s,FI}} & \boldsymbol{\Phi}_{\mathrm{s,FF}} \end{bmatrix} \begin{bmatrix} \boldsymbol{r}_{\mathrm{s,I}} \\ \boldsymbol{u}_\mathrm{d} \end{bmatrix} = \boldsymbol{\Gamma}_\mathrm{s}\, \boldsymbol{q}_\mathrm{s} \quad (2)$$

for the structural domain and

$$\begin{bmatrix} \boldsymbol{p}_\mathrm{I} \\ \boldsymbol{p}_\mathrm{F} \end{bmatrix} = \begin{bmatrix} \boldsymbol{\Delta}_\mathrm{a} & \boldsymbol{0} \\ -\boldsymbol{K}_{\mathrm{a,FF}}^{-1}\boldsymbol{K}_{\mathrm{a,FI}} & \boldsymbol{\Phi}_{\mathrm{a,FF}} \end{bmatrix} \begin{bmatrix} \boldsymbol{r}_{\mathrm{a,I}} \\ \boldsymbol{p}_\mathrm{d} \end{bmatrix} = \boldsymbol{\Gamma}_\mathrm{a}\, \boldsymbol{q}_\mathrm{a} \quad (3)$$

for the acoustic domain, respectively. Hereby, index "F" stands for inner DOFs, whereas index "I" characterizes interface DOFs. The described reduction basis reduces the coupled system to $nc \ll n$ DOFs. The coupling between the reduced component models is defined by single point contraints at the component interface. This holds for both the solid and the fluid domain, and implicit scleronomic coupling conditions are established. They are used for the generation of an explicit transformation matrix $\mathbf{Q}$ from component coordinates in coordinates of the assembled piping system [2] which allows the subsequent summation of n substructure contributions

$$\underbrace{\sum_{i=1}^{n}\begin{bmatrix} \boldsymbol{Q}_{\mathrm{s},i}^{\mathrm{T}}\boldsymbol{M}_{\mathrm{s},i}^{\diamond}\boldsymbol{Q}_{\mathrm{s},i} & \mathbf{0} \\ \rho\boldsymbol{Q}_{\mathrm{a},i}^{\mathrm{T}}\boldsymbol{C}_{i}^{\diamond}\boldsymbol{Q}_{\mathrm{s},i} & \boldsymbol{Q}_{\mathrm{a},i}^{\mathrm{T}}\boldsymbol{M}_{\mathrm{a},i}^{\diamond}\boldsymbol{Q}_{\mathrm{a},i} \end{bmatrix}}_{\boldsymbol{M}_{\mathrm{g}}} \begin{bmatrix} \ddot{\boldsymbol{q}}_{\mathrm{s}} \\ \ddot{\boldsymbol{q}}_{\mathrm{a}} \end{bmatrix}$$
$$+\underbrace{\sum_{i=1}^{n}\begin{bmatrix} \boldsymbol{Q}_{\mathrm{s},i}^{\mathrm{T}}\boldsymbol{K}_{\mathrm{s},i}^{\diamond}\boldsymbol{Q}_{\mathrm{s},i} & -\boldsymbol{Q}_{\mathrm{s},i}^{\mathrm{T}}\boldsymbol{C}_{i}^{\diamond}\boldsymbol{Q}_{\mathrm{a},i} \\ \mathbf{0} & \boldsymbol{Q}_{\mathrm{a},i}^{\mathrm{T}}\boldsymbol{K}_{\mathrm{a},i}^{\diamond}\boldsymbol{Q}_{\mathrm{a},i} \end{bmatrix}}_{\boldsymbol{K}_{\mathrm{g}}} \begin{bmatrix} \boldsymbol{q}_{\mathrm{s}} \\ \boldsymbol{q}_{\mathrm{a}} \end{bmatrix}$$
$$= \sum_{i=1}^{n}\begin{bmatrix} \boldsymbol{Q}_{\mathrm{s},i}^{\mathrm{T}}\boldsymbol{f}_{\mathrm{s},i} \\ \boldsymbol{Q}_{\mathrm{a},i}^{\mathrm{T}}\boldsymbol{f}_{\mathrm{a},i} \end{bmatrix}, \qquad (4)$$

where $\boldsymbol{M}_{\mathrm{s}}^{\diamond} = \boldsymbol{\Gamma}_{\mathrm{s}}^{\mathrm{T}}\boldsymbol{M}_{\mathrm{s}}\boldsymbol{\Gamma}_{\mathrm{s}}$, $\boldsymbol{M}_{\mathrm{a}}^{\diamond} = \boldsymbol{\Gamma}_{\mathrm{a}}^{\mathrm{T}}\boldsymbol{M}_{\mathrm{a}}\boldsymbol{\Gamma}_{\mathrm{a}}$, $\boldsymbol{K}_{\mathrm{s}}^{\diamond} = \boldsymbol{\Gamma}_{\mathrm{s}}^{\mathrm{T}}\boldsymbol{K}_{\mathrm{s}}\boldsymbol{\Gamma}_{\mathrm{s}}$, $\boldsymbol{K}_{\mathrm{a}}^{\diamond} = \boldsymbol{\Gamma}_{\mathrm{a}}^{\mathrm{T}}\boldsymbol{K}_{\mathrm{a}}\boldsymbol{\Gamma}_{\mathrm{a}}$, $\boldsymbol{C}^{\diamond} = \boldsymbol{\Gamma}_{\mathrm{a}}^{\mathrm{T}}\boldsymbol{C}\boldsymbol{\Gamma}_{\mathrm{s}}$, $\boldsymbol{f}_{\mathrm{s}} = \boldsymbol{\Gamma}_{\mathrm{s}}^{\mathrm{T}}\boldsymbol{f}$, and $\boldsymbol{f}_{\mathrm{a}} = \boldsymbol{\Gamma}_{\mathrm{a}}^{\mathrm{T}}\boldsymbol{q}$.

A detailed description of the substructuring technique and a way how to avoid locking problems for the applied interface reduction are presented in [3]. In the present work, a water-filled piping system with a cross section change is assembled using three substructures. The reduced system has $nc = 389$ DOFs as opposed to $n = 8762$ DOFs of the full FE model. The first superelement is a straight pipe section (length 0.263 m) with an outer radius of 3 mm and a wall thickness of 0.7 mm. The second substructure is characterized by a cross section change as depicted in Fig. 1. The third component is another straight pipe section (length 0.306 mm) with the same uniform cross section as the first substructure and a closed end. To achieve a compatible mesh between the component interfaces, the substructure with the small inner pipe radius includes a thin element layer at both ends to enable the transition between the two different pipe diameters as depicted in Fig. 1. The piping system is clamped on the left end and an acoustic pressure excitation is applied as boundary condition.

Fluid Damping Model

So far, no damping has been considered. This section describes how a fluid damping model is integrated in the finite element based component synthesis described above. The frequency dependent fluid damping model according to Theissen [4] is based on a complex wave number

$$\kappa_{1,2} = \pm\sqrt{-\frac{J_0(r^*)}{J_2(r^*)}}\frac{\mathrm{i}\omega}{c}, \qquad (5)$$

with $r^* = \mathrm{i}\sqrt{\frac{\mathrm{i}\omega}{\nu}}r$. Note that r^* is as a normalized form of the inner pipe radius r, whereas c is the speed of sound and J_0, J_2 are Bessel functions of first kind and 0th and 2nd order, respectively. The damped 1D wave equation is given as

$$\nabla^2 p + \frac{4\nu}{3c^2}\frac{\partial}{\partial t}\nabla^2 p - \frac{1}{c^2}\frac{\partial^2 p}{\partial t^2} = 0, \qquad (6)$$

whereas the viscous term $\frac{4\nu}{3c^2}$ is written as β_v in the following. In the frequency domain, the wave equation is defined as

$$\nabla^2 p + \frac{1}{c^2\left(1+\mathrm{i}\omega\beta_v\right)}\omega^2 p = 0 \qquad (7)$$

and a complex circular wave number is derived as

$$\kappa = \frac{\omega}{c}\frac{1}{\sqrt{1+\mathrm{i}\omega\beta_v}}. \qquad (8)$$

In the next step, the negative real part of κ is equated with its counterpart of Eq. 5 (following the Ansatz $p(x) = Ae^{\kappa x}$) and the damping parameter β_v is computed from this simplified approach. Since the viscous term β_v depends on the inner pipe radius and wall friction effects (which is the dominant damping mechanism in thin pipes), local damping effects due to the cross section change are modeled in an appropriate manner. Stiffness proportional damping is assumed and the fluid damping model is integrated in the finite element model of each substructure. The global viscous damping matrix is assembled by

$$\boldsymbol{D}_{\mathrm{g}} = \sum_{i=1}^{n}\begin{bmatrix} \boldsymbol{D}_{\mathrm{s},i} & \mathbf{0} \\ \mathbf{0} & \boldsymbol{D}_{\mathrm{a},i} \end{bmatrix}$$

with

$$\boldsymbol{D}_{\mathrm{a},i}(\omega) = \beta_{v,i}(\omega)\boldsymbol{Q}_{\mathrm{a},i}^{\mathrm{T}}\boldsymbol{K}_{\mathrm{a},i}^{\diamond}\boldsymbol{Q}_{\mathrm{a},i}. \qquad (9)$$

The fluid damping matrix is computed for each frequency step during the harmonic analysis. The viscous term $\beta_{v,i}$ is computed for each individual substructure (denoted as "Theissen local" in the results section). Thus, the local damping effect of the orifice is captured by the proposed damping model. It is worth noting, that the computation of the damping matrix only at eigenfrequencies of each substructure is not meaningful since the first eigenfrequency of the small component with the orifice lays beyond the frequency range of interest. Thus, the influence of this substructure on the damping behavior of the assembled piping system is not captured in a suitable manner. An alternativ modal approach considers the viscous damping only at the eigenfrequencies of the assembled piping system (denoted as "Theissen modal"). Hereby, local damping effects due to the cross section change are not included, but for piping systems with a uniform cross section, the modal approach gives excellent results [5] since wall friction effects are also included.

The structural partition of the global damping matrix is given as

$$\boldsymbol{D}_{\mathrm{s},i} = \alpha_{\mathrm{s},i}\boldsymbol{Q}_{\mathrm{s},i}^{\mathrm{T}}\boldsymbol{M}_{\mathrm{s},i}^{\diamond}\boldsymbol{Q}_{\mathrm{s},i} + \beta_{\mathrm{s},i}\boldsymbol{Q}_{\mathrm{s},i}^{\mathrm{T}}\boldsymbol{K}_{\mathrm{s},i}^{\diamond}\boldsymbol{Q}_{\mathrm{s},i}, \qquad (10)$$

assuming a Rayleigh damping model for each substructure. Eq. 4 can now be augmented by the global viscous damping matrix and the harmonic analysis is performed for the gobal system in order to obtain the hydraulic transfer function.

Experimental Setup

The experimental setup of the hydraulic test bench is illustrated in Fig 2. The setup consists of a hydroacoustic pressure source and a steel pipe (E=206 GPa, ρ_s=7900 kg/m^3, total length 0.55 m) filled with water (c = 1460 m/s, ρ_a=1000 kg/m^3). The pipe is characterized by a cross section change due to an orifice with a length of 2 mm. The pressure source consists of two piezostacks which are arranged perpendicularly to the direction of wave propagation and on opposite sides of the hydraulic pipe. The piezostacks are driven by a power amplifier and a function generator and oscillate with opposite phase in order to excite pressure pulsations in the fluid column [5]. The supply pipe with the additional pump is required to fill and compress the fluid to ensure a stable fluid column without any air bubbles, which is a challenging task especially for small orifice diameters. The dynamic pressure pulsations are measured with piezoelectric pressure sensors.

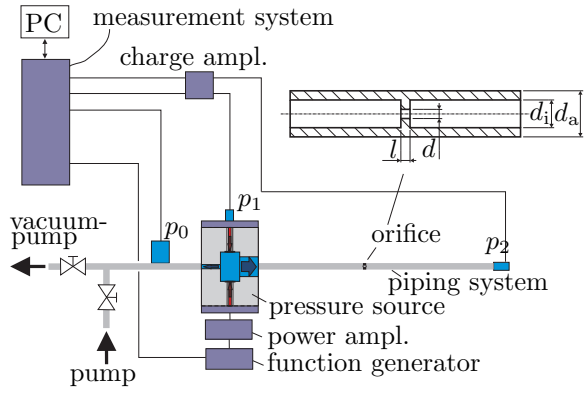

Figure 2: Experimental setup of the hydraulic test bench.

Hydroacoustic Excitation

A sweep excitation is chosen in order to excite a wide frequency range. The repeated sweep signals have a cycle duration of 200 ms. A typical time signal of the inlet pressure p_1 and the corresponding FFT is depicted in Fig. 3. 15 swept pressure signals are averaged in order to estimate the hydraulic transfer function between the pressure at the beginning and at the end of the pipe using the Matlab function "tfestimate".

Cross Section Changes

Three different cross section changes are analyzed in this research. Appropriate orifices are integrated in the piping system to obtain the cross section change of interest. The inner pipe diameters d of the different orifices are 1.2 mm, 0.9 mm and 0.6 mm, whereas the inner pipe diameter of the long pipe sections before and after the orifice is d_i = 4.6 mm. The length of the orifice is kept constant to l = 2 mm.

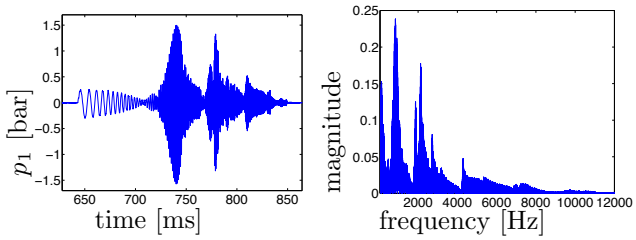

Figure 3: Typical swept time signal (left) and FFT of the input pressure p_1.

Results

Hydraulic Transfer Function

The hydraulic transfer function $H_{p1\to p2}$ is measured using the hydraulic test bench and the result is compared to the finite element simulation using the substructuring technique as described before. The result of the hydraulic or hydroacoustic transfer function for the pipe with an orifice diamter of d = 1.2 mm is shown in Fig. 4. The coherence of the measurement is plotted in the same figure. The correlation between experiment and simulation is very good, both for the hydraulic resonances and the predicted damping. A kinematic viscosity of $\nu = 0.75 \cdot 10^{-6}$ m^2/s is assumed for the fluid damping model. From the figure it seems that the local and modal Theissen model give almost the same results, but a closer look at the peak values reveals that the local model (dashed curve) leads to a better correlation with the measurement. Thus, only the local fluid damping model is used in the following.

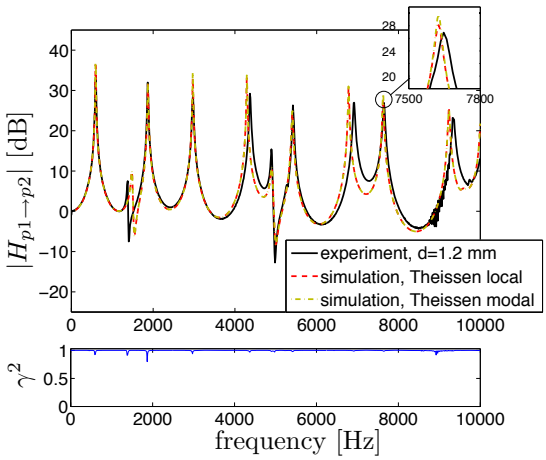

Figure 4: Hydraulic transfer function: comparison between experiment and simulation using the damping model "Theissen local" and "Theissen modal"; orifice diameter: 1.2 mm.

Influence of Diameter Changes

The influence of the orifice diameter on the hydraulic resonances and the observed damping is clearly visible in Fig. 5. The larger the cross section change (and the smaller the orifice diameter d), the smaller the resonance peaks. The hydraulic resonance frequencies are shifted to lower frequencies due to the increasing hydraulic inertia for decreasing orifice diameters (added mass effect). Fig. 6 and Fig. 7 show the hydraulic

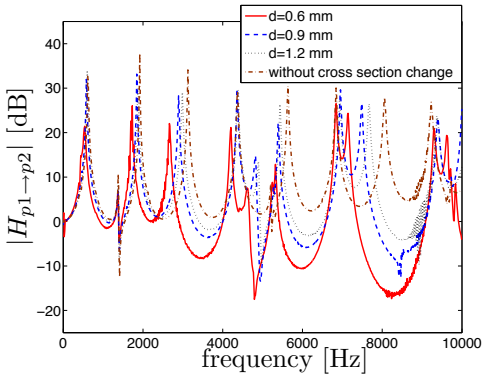

Figure 5: Measured hydraulic transfer function of pipes with different orifice diameters and comparison with a pipe without cross section change.

transfer function for orifice diameters $d = 0.9$ mm and $d = 0.6$ mm, respectively. Again, the correlation between experiment and simulation is very good for almost the entire frequency range up to 8 kHz except the peak values for the pipe with the largest cross section change ($d = 0.6$ mm). The noisy part of the measured transfer function around 8.3 kHz is due to the eigenfrequency of the piezo stack-acktuator. Two coupled modes are visible where a structural resonance of the pipe shell interacts with the acoustic fluid. The first coupled peak around 1.5 kHz is characterized by a longitudinal mode of the pipe structure. The second coupled mode with the typical antiresonance behavior around 5 kHz strongly depends on the pipe section with the orifice.
Note that the mean flow velocity is neglected in this research since the superimposed mean flow is very small when compared with the hydroacoustic speed (Mach number $M << 1$) [2]. Nonlinear flow–related effects may occur if the excitation level is further increased. The unsteady orifice behavior to describe the attenuation of oscillating pressure pulsations is investigated in [8].

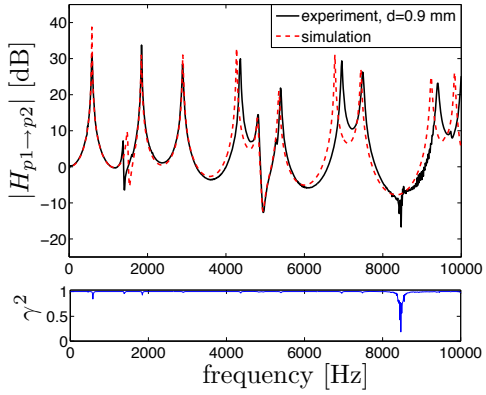

Figure 6: Hydraulic transfer function: comparison between experiment and simulation for an orifice diameter of 0.9 mm.

Conclusion

The influence of a cross section change on the dynamic behavior of a fluid-filled piping system is analyzed in this research using a hydraulic test bench and an efficient finite element based substructuring technique. A cross section change due to an orifice leads to a local damping

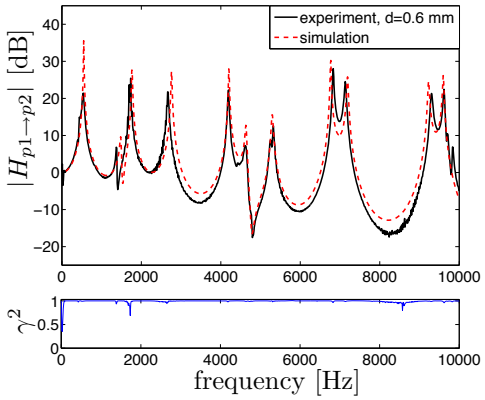

Figure 7: Hydraulic transfer function: comparison between experiment and simulation for an orifice diameter of 0.6 mm.

effect and a frequency shift of the hydraulic resonances. A local, frequency dependent fluid damping model is successfully integrated in the substructuring technique and gives promising results.

Acknowledgments

The authors wish to thank Dr.-Ing. Matthias Maess and Dipl.-Ing. Jürgen Koreck at Robert Bosch GmbH for their help and advice.

References

[1] R.R. Craig, M.C.C. Bampton, "Coupling of substructures for dynamic analysis", *AIAA Journal* **6**, 1313-1319 (1968).

[2] M. Maess, "Methods for Efficient Acoustic-Structure Simulation of Piping Systems", Ph.D. thesis, Institute of Applied and Experimental Mechanics, University of Stuttgart, 2006.

[3] J. Herrmann, M. Maess, L. Gaul, "Efficient Substructuring Techniques for the Investigation of Fluid-Filled Piping Systems", In: *Proceedings of IMAC-XXVII*, Orlando, 2009.

[4] H. Theissen, "Die Berücksichtigung instationärer Rohrströmung bei der Simulation hydraulischer Anlagen", Ph.D. thesis, RWTH Aachen, 1983.

[5] J. Herrmann, T. Haag, L. Gaul. K. Bendel, H.-G. Horst, "Experimentelle Untersuchung der Hydroakustik in Kfz-Leitungssystemen", In: *Proceedings of DAGA*, Dresden, 2008.

[6] O. Zienkiewicz, R. Taylor, *The Finite Element Method*, Butterworth-Heinemann, Oxford, 2000.

[7] R.R. Craig, C.J. Chang: Substructure coupling for dynamic analysis and testing, *NASA CR 2781*, 1977.

[8] J. Koreck, O. von Estorff: Frequency Dependent Attenuation of Oscillations in Fluid-filled Pipes and Orifices, In: *Proceedings of NAG/DAGA*, Rotterdam, 2009.